

Couette Flow of Two-Dimensional Foams

GIJS KATGERT¹, BRIAN P. TIGHE², MATTHIAS E. MÖBIUS¹ and MARTIN VAN HECKE¹

¹ *Kamerlingh Onnes Laboratorium, Universiteit Leiden, P.O. Box 9504, 2300 RA Leiden, The Netherlands.*

² *Instituut Lorentz, Universiteit Leiden, P.O. Box 9506, 2300 RA Leiden, The Netherlands.*

PACS 47.57.Bc – Foams and emulsions
 PACS 83.60.Fg – Shear rate-dependent viscosity
 PACS 83.80.Iz – Emulsions and foams
 PACS 83.10.Gr – Constitutive relations

Abstract. - We experimentally investigate flow of quasi two-dimensional disordered foams in Couette geometries, both for foams squeezed below a top plate and for freely floating foams (bubble rafts). With the top plate, the flows are strongly localized and rate dependent. For the bubble rafts the flow profiles become essentially rate-independent, the local and global rheology do not match, and in particular the foam flows in regions where the stress is below the global yield stress. We attribute this to nonlocal effects and show that the “fluidity” model recently introduced by Goyon *et al.* (*Nature*, **454** (2008)) captures the essential features of flow both with and without a top plate.

Introduction. – Foams have recently attracted attention as model systems for disordered, complex fluids [1]. The elementary building blocks, the bubbles, obey simple laws: when compressed, their repulsion is harmonic [2, 3] and when sliding past other bubbles or boundaries, they experience a velocity dependent drag force [4–10].

Collectively, the conglomerate of bubbles that makes up a foam exhibits all the hallmarks of complex fluids — foams exhibit shear banding, a yield stress and shear-thinning [11]. The latter are often modeled by a Herschel-Bulkley constitutive equation where the stress τ takes the form $\tau = \tau_y + k\dot{\gamma}^\beta$, where τ_y, k, β and $\dot{\gamma}$ denote the yield stress, consistency, power law index and strain rate [11].

The rheology of foams has mainly been investigated in three dimensions [1]. While the three-dimensional case is perhaps more realistic, the opacity of foams inhibits connecting the bulk behavior with the local behavior. Therefore, recently a body of work has focused on the shear flow of two dimensional foams. In this case the bulk response can easily be connected to local quantities such as velocity profiles and bubble fluctuations [12–14].

The flow of two dimensional foams has been studied extensively in Couette geometries. For example, Dennin and co-workers have sheared (freely floating) bubble rafts in a Couette geometry with a fixed inner disk and a rotating outer cylinder [15, 16], while Debrégeas has con-

finned foam bubbles in a Hele-Shaw cell and rotated the inner disk, keeping the outer cylinder fixed [17]. In both cases, localized flow profiles were found. There has been no clear consensus, however, on the cause of flow localization in these systems: while the (geometry induced) decay of the stress away from the inner cylinder may cause localization, a confining glass boundary, by introducing additional drag forces on the foam, can have the same effect [12, 18–20]. Thus the question of what causes flow localization remains, and differing opinions abound in the community [21–23].

In this Letter, we address this question by combining measurements of the flow profiles of two-dimensional disordered foams in Couette geometries with and without a top plate and for a wide range of driving rates with independent rheological measurements. When the top plate is present the flows are rate dependent, while the flow profiles become essentially rate-independent in absence of this plate — in both cases, the flow profiles are localized.

A recent model, developed by Janiaud *et al.* and Katgert *et al.* successfully predicts velocity profiles in *linearly* sheared monolayers [12, 24] by balancing a Herschel-Bulkley expression for the stress with a drag force due to the top plate. Here we show that this model unexpectedly breaks down in Couette geometries [19]. This is seen most dramatically in the case without a top plate, where, due

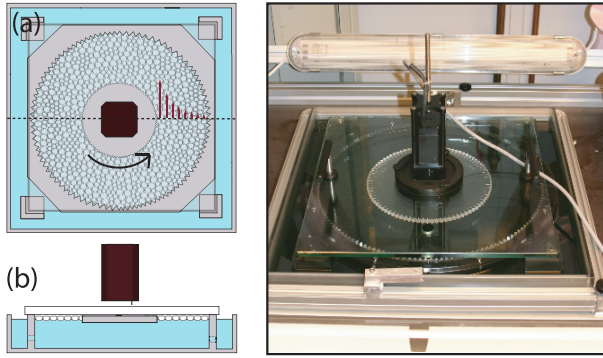


Fig. 1: (a) Schematic top view of one Couette cell used in this experiment. The inner disk has radius $r_i = 105$ mm and the gap has width 85 mm. The outer cylinder, reservoirs and supports for the glass plate have been milled into a PMMA block. (b) Side view: the reservoirs and the bounded area are connected to keep the region underneath the glass plate from draining. The motor is connected to the inner cylinder through the glass plate. (c) Photograph of the experimental setup.

to the presence of a yield stress, Herschel-Bulkley rheology predicts a range of driving rates for which the flow velocity vanishes at a point *within* the gap. In these cases, we observe instead a velocity profile that decays to zero only at the outer boundary. Thus, the material appears to flow below the yield stress! Moreover, the Herschel-Bulkley constitutive relation fails to capture the observed rate independence.

Thus, the Herschel-Bulkley model fails to capture the flow, and we show that this breakdown reflects nonlocal flow behavior. By applying the nonlocal model recently introduced by Goyon *et al.* [25,26], which contains a finite cooperativity length ξ that encodes the spatial extent of plastic rearrangements, we find that we can describe all features of the flow of foam in Couette geometry.

Experiment. – Our experimental setup consists of a $500 \times 500 \times 50$ mm square PMMA block, into which the outer cylinder, a reservoir and supports for a removable glass plate are milled, see Fig. 1. The boundary of the reservoir acts as the outer cylinder (of radius $r_o = 190$ mm) and is grooved with 6 mm grooves. On the glass plate of $405 \times 405 \times 12$ mm, a casing for a stepper motor is fixed by UV curing glue. The stepper motor (L-5709 Lin engineering) is connected to an inner cylinder of $r_i = 105$ mm radius through a hole in the glass plate. The inner cylinder is grooved like the outer cylinder.

A bidisperse foam is produced by filling the reservoir with a surfactant solution, the details of which can be found in [12] and bubbling nitrogen through the fluid (viscosity $\eta = 1.8 \pm 0.1$ mPa·s and surface tension $\sigma = 28 \pm 1$ mN/m) [12]. After thorough mixing, we obtain a bidisperse, disordered foam monolayer. The resulting bubble sizes are $d_1, d_2 = 1.8, 2.7$ mm. The glass plate, with the inner driving wheel attached, is carefully placed on top of the foam and subsequently, the foam is allowed to equi-

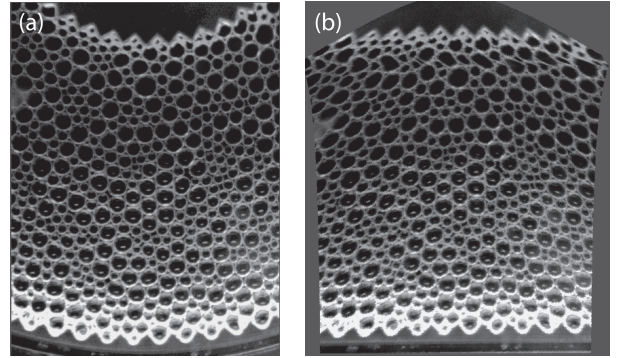


Fig. 2: (Color online) (a) Raw image as obtained by CCD camera. The local curvature is extracted from the curvature at the inner disk and the outer cylinder, and for every r we define an arc that we match to pixels in the image. If we plot these arcs as straight lines we obtain: (b) the image with correction for curvature. We compute cross correlations between subsequent frames on these straightened image lines.

brate for a considerable time. Approximately 40 bubble layers span the distance between the inner wheel and the outer cylinder. To perform bubble raft experiments, we place spacers between the supports and the glass plate, thus obtaining a considerable gap between the liquid surface and the glass plate.

The foam is lit laterally by 4 fluorescent tubes and images are recorded by a CCD camera (Foculus FO 432BW), equipped with a Tamron 280-300 telezoom lens. The bottom of the reservoir is black to enhance contrast. The frame rate is fixed such that the angular displacement of the inner cylinder is fixed at 1.12×10^{-3} rad/frame. We record only during steady shear, ensuring that the foam has been sheared considerably before starting image acquisition.

We calculate velocity profiles across the gap between inner and outer wheel by cross-correlating arcs of fixed radial distance in subsequent frames over a large angular region. This approach forces us to calculate velocity profiles on curved image lines. However, by defining circular arcs and identifying these with the appropriate pixels, this can easily be done, see Fig. 2(a,b). We compute averaged velocities over between 2,000 and 10,000 frames, depending on the experiments, to enhance statistics. We assume the accuracy of the profiles to be at best 0.001 pixel/frame and cut off velocities that fall below this threshold. We check that coarsening, segregation, coalescence and rupturing are absent in the runs with a top plate, whereas we do observe rupturing in the bubble raft experiment: bubbles will pop after approximately $1\frac{1}{2}$ hours. We merely content ourselves with the absence of holes in our foam during the latter experiment, which is achieved by loading the Couette cell with a surplus of foam far away from the imaging region.

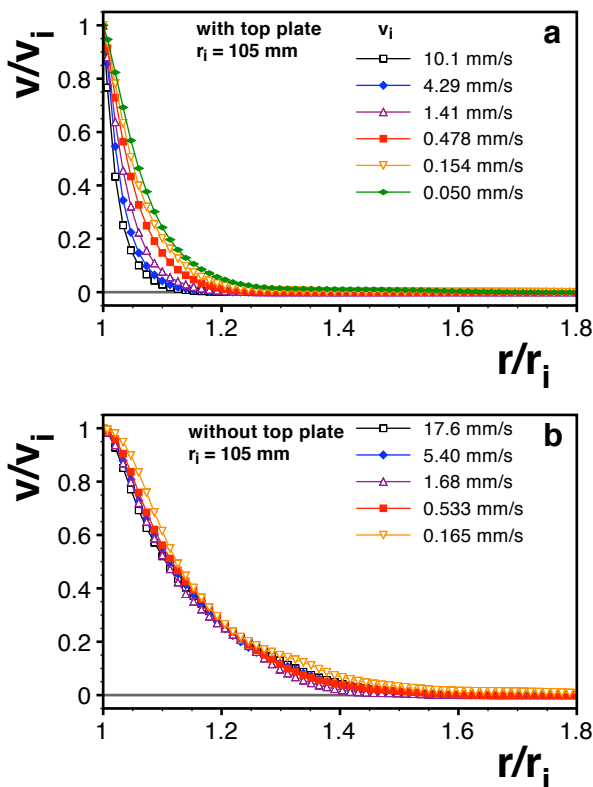


Fig. 3: (Color online) (a) Velocity profiles for two dimensional Couette flow of foam with top plate. We see strongly localized velocity profiles that furthermore exhibit rate dependence: the faster the driving velocity v_i , the more localized the profiles become. (b) Velocity profiles for two dimensional Couette flow of foam without top plate. We see approximately rate independent velocity profiles, with localization that is solely due to the curved geometry.

Results. – In Fig. 3(a) we present data for the shear flow of a foam covered with a glass plate, at 6 different driving velocities $v_i := v(r_i)$ spanning 2.5 decades. We have rescaled the velocity profiles with v_i to highlight the qualitative changes and we have rescaled the radial coordinate with the inner radius r_i , which characterizes the curvature of the experimental geometry and, in the case without a top plate, sets the decay of the stress profile. We observe that the shape of the velocity profiles depends on the exerted rate of strain; the runs that were recorded at the highest driving velocity exhibit the most localization.

The observed rate dependence is in accordance with our previous results [12], obtained for the linear shear of two-dimensional foams bounded by a top plate, which also displayed rate dependent localization in the presence of a top plate. From these results, we can infer that again the balance between internal dissipation in the foam and the external top plate drag force leads to increased localization at increasing shear rates. Note that our results are in strong contrast with the findings by Debrégeas et al. [17], where rate independent profiles were found. As in [17], the

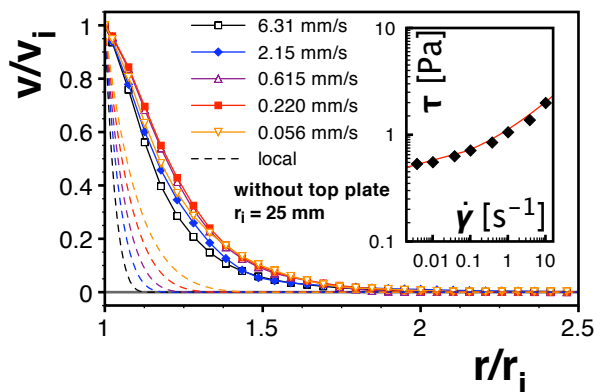


Fig. 4: Data from liquid-air Couette geometry with inner disk of radius $r_i = 25$ mm driven by rheometer head. Averaged and normalized velocity profiles for a range of driving velocities v_i at the inner disk. Dashed lines: Flow profiles for a fluid obeying a Herschel-Bulkley constitutive relation. The HB parameters are determined from rheometric data shown in the inset. Black squares: Shear stress τ_i versus strain rate $\dot{\gamma}$ measured at the inner disk. Red curve: Fit to a Herschel-Bulkley constitutive relation $\tau = \tau_y + k\dot{\gamma}^\beta$ with $\tau_y = 0.42$ Pa, $\beta = 0.36$, and $k = 0.7$ Pa \cdot s $^{1/\beta}$.

decay of the velocity profile is approximately exponential (semi-log plot not shown).

We now turn to Couette shear of a freely flowing foam without drag from the top plate. Despite the limited stability of the bubble raft, we can shear the foam at the same shear rates as in the experiments with a bounding glass plate, except for the slowest run. Results are plotted in Fig. 3(b): within experimental uncertainty the profiles exhibit rate independent velocity profiles. We observe that the velocity profiles are still reasonably localized.

Localization absent the top plate is not itself surprising: Herschel-Bulkley fluids are expected to display localization in Couette flow when the shear stress, which decays as $1/r^2$, falls below the yield stress. At this point, the local strain rate is discontinuous. Here we do not observe any such discontinuity in the local strain rate. This should be contrasted to earlier claims of flow discontinuities by Rodts et al. [27] and Dennin and co-workers [16, 23, 28] experimentally and Cheddadi et al. theoretically [21]. We note here that the experimental proof of a flow discontinuity is highly non-trivial — that is why we turn our attention to rheometry. We have not seen packing density gradients associated with the flow localization, and gradients are smooth enough (except very close to the wall), to exclude effects due to the discrete nature of the material [29].

Rheometry. – We now directly investigate the applicability of a local rheology for the flow of a bubble raft, i.e. in the absence of a top plate. To do so, we have performed additional measurements by simultaneously imaging the velocity profiles and measuring the bulk rheometri-

cal response of a two dimensional bubble raft in a Couette geometry. This allows us to investigate the local rheology of the foam in the spirit of [25, 26] and connect bulk rheometry with local measurements, as well as model solutions.

We shear the bubble raft in an Anton Paar DSR 301 rheometer. We employ a Couette geometry, now with inner disk and outer ring radii of $r_i = 25$ mm and $r_o = 73$ mm. We impose five different strain rates spanning two decades and measure the resulting averaged torque, while simultaneously imaging the bubble motion. The measured flow profiles and rheology are shown in Fig. 4. Note that, to within experimental scatter and similar to the Couette flows of bubble rafts with the larger inner disk, shown in Fig. 3b, the profiles are rate independent.

An advantage of omitting the top plate is that we can determine the stress $\tau(r)$ from the torque on the inner disk, which is connected to the rheometer head. When there is no top plate, the shear stress satisfies $\frac{1}{r^2} \frac{\partial}{\partial r} (r^2 \tau) = 0$, hence $\tau(r) = \tau_i (r_i/r)^2$. From the measured velocity profile, the local strain rate can be obtained as $\dot{\gamma} = \frac{\partial v(r)}{\partial r} - \frac{v(r)}{r}$. The inset of Fig. 4 plots stress versus strain rate at the inner disk. The experimental stress-strain rate data is consistent with a Herschel-Bulkley constitutive relation with a yield stress of $\tau_y = 0.42$ Pa, rheological exponent of $\beta = 0.36$, and consistency $k = 0.7$ Pa \cdot s $^{1/\beta}$. This flow curve is consistent with earlier measurements [12, 13].

Equipped with a constitutive relation, we can now calculate the expected flow profiles for given experimental parameters. We solve for the flow profile $v(r)$ subject to the imposed driving velocity $v(r_i) = v_i$ and no-slip boundary conditions $v(r_o) = 0$ at the outer wall; results are plotted in Fig. 4. The Herschel-Bulkley flow profiles are noticeably more shear banded than the experimental profiles and, unlike the data, display rate dependence. Flow ceases at the point where the stress $\tau(r)$ decays below τ_y ; this occurs at a position within the gap and is clearly visible in Fig. 4. Therefore the flow profiles predicted on the basis of the constitutive relation determined from rheometry and imaging fail dramatically. We now show that this departure is due to nonlocal rheology.

Nonlocal effects. – Because we access velocity profiles in addition to rheometric data, we know the mean strain rate and mean shear stress at every point within the gap, for the case without a top plate. It is thus possible to make parametric plots in which the radial coordinate is varied, as shown in Fig. 5a. This is equivalent to plotting a constitutive relation for each radial coordinate within the gap.

Fig. 5a demonstrates two things. First, the absence of a collapse of the parametric plots for the five different runs clearly shows that there is no local rheology — for a single given local stress, a range of local strain rates can be obtained. If the rheology were local, all data would collapse to a master curve, e.g. a Herschel-Bulkley or other constitutive relation. Second, we find that there can be flow

($\dot{\gamma} > 0$) in the wide-gapped Couette geometry for shear stresses *below* the rheometrically determined global yield stress, $\tau(r) < \tau_Y$. This cannot occur within a material that is locally described by the Herschel-Bulkley constitutive relation. Each parametric curve terminates on the stress-strain rate curve of Fig. 4 (inset) because the curve was measured at the inner wheel.

We will now show that a simple nonlocal model recently developed by Goyon *et al.* can capture the flow of a bubble raft. This nonlocal model proposes that a material’s local propensity to flow, characterized by the fluidity, can be influenced by flow elsewhere in the material.

Model. – The key ingredient of the nonlocal model is the position-dependent inverse viscosity, or “fluidity”, $f := \dot{\gamma}/\tau$, a measure of the material’s tendency to flow. To obtain an equation for the fluidity, one can argue as follows. A system with homogeneous stress and strain rate is characterized by the “bulk fluidity”

$$f_b := \frac{\dot{\gamma}_{HB}}{\tau} = \frac{1}{\tau} \left(\frac{\tau - \tilde{\tau}_y}{\tilde{k}} \right)^{1/\tilde{\beta}} \Theta(\tau - \tilde{\tau}_y). \quad (1)$$

$\Theta(x)$ is the unit step function. The tilde indicates that parameters may, in principle, differ from the “wall constitutive relation” of Fig. 4 (inset). The key idea is that, in the presence of inhomogeneity, the system “wants” to achieve a fluidity $f = f_b$ everywhere, i.e. to obey local rheology, but is forced to pay a price for spatial variations in f . Writing in one dimension for simplicity, these ideas can be expressed very generally in integral form: $f_b(x) = \int dx' K(x, x') f(x')$. The kernel $K(x, x') = K(x - x')$ must be a symmetric function of the distance between two points. K must further satisfy $\int ds K(s) = 1$ to recover the bulk fluidity f_b in a homogeneous system. Taylor expanding f in the integrand to second order in s yields:

$$f_b(x) = f(x) - \xi^2 \frac{\partial^2}{\partial x^2} f(x). \quad (2)$$

The parameter $\xi^2 := -\int ds s^2 K(s)$ sets a length scale, termed the cooperativity length, that characterizes nonlocal effects [30]. Here, as in [25], we take it as a fitting parameter.

Note that the diffusive term in Eq. (2) is in some sense the simplest possible realization of a nonlocal model for the fluidity. For the Couette geometry we employ cylindrical coordinates and let $\frac{\partial^2}{\partial x^2} \rightarrow \frac{1}{r} \frac{\partial}{\partial r} (r \frac{\partial}{\partial r})$.

Boundary conditions on the fluidity are required: we impose $f_i = \tau_i^{-1} [(\tau_i - \tau_y)/k]^{1/\beta}$ at the inner wheel, with parameters from the wall constitutive relation, and $f_o = 0$ at the outer ring. Parameters in the bulk fluidity, Eq. (1), must also be specified. In the experiments on emulsions of [25], where it was possible to access these parameters independently, it was found that $\tilde{\tau}_y = \tau_y$ and $\tilde{\beta} = \beta$. For smooth walls $\tilde{k} = k$, while for rough walls \tilde{k} was smaller by roughly a factor one half. For the results we present here,

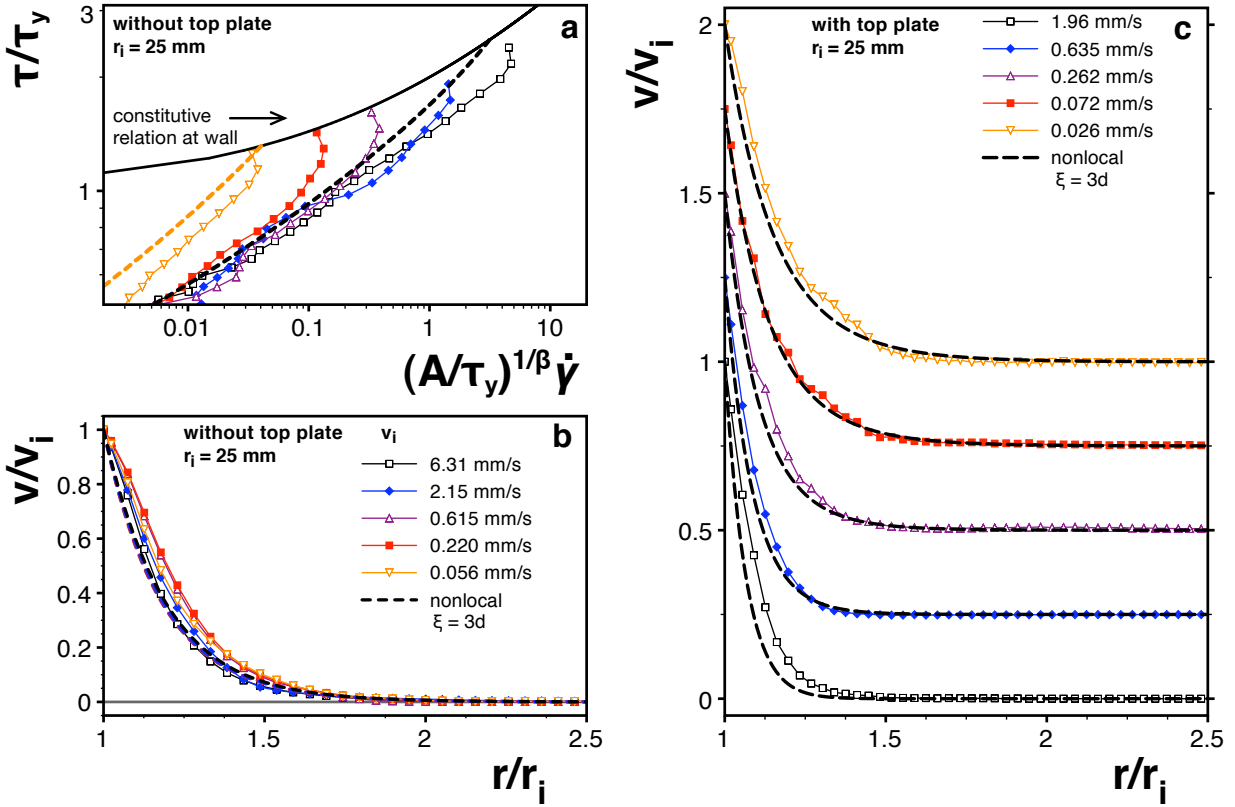


Fig. 5: Nonlocal rheology of foams. (a) Data points: local flow curves in the Couette geometry without a top plate. The local strain rate can be calculated from the velocity profiles in Fig. 4 and the stress at the inner disk known from the measured torque. Different colors correspond to different driving velocities (legend as in (b)); for a given driving velocity, different points correspond to different positions in the gap. Solid curve: The “wall constitutive relation” shown in Fig. 4 (inset). Dashed curves: Predictions of the nonlocal model with cooperativity length $\xi = 3\langle d \rangle$. We plot only the curves for the slowest and fastest driving rates. (b) Data points: Identical to the data of Fig. 4 for flow without a top plate. Dashed curves: Predictions of the nonlocal model. The model yields near rate independence; the five plotted curves lie nearly on top of one another. (c) Data points: Velocity profiles for the system with $r_i = 25$ mm and a top plate. Dashed curves: Predictions of the nonlocal model for the identical set of parameters used in (b). Curves are offset for clarity.

varying \tilde{k} over this range does not substantially alter the quality of agreement between theory and experiment, both for flow curves and velocity profiles. Hence we set $\tilde{k} = k$ for simplicity, i.e. we take the bulk and wall fluidities to be identical. Once Eq. (2) has been solved for f , the velocity profile can be integrated by assuming no slip, $v(r_o) = 0$, at the outer ring.

Flows without a top plate. For the bulk fluidity we use the Herschel-Bulkley parameters determined by fitting to the rheometrical data in the inset of Fig. 4. We then vary ξ and obtain a good match with the data for $\xi/\langle d \rangle = 3 \pm 0.5$. As shown in Fig. 5b, the flow profiles predicted by this model are qualitatively similar to those measured, and show very little rate dependence. In particular, the model correctly captures the presence of flow in regions where the local stress is below the yield criterion of the local model; this flow is induced by cooperative effects, apparently well-captured by the nonlocal model.

As illustrated in Fig. 5a, this nonlocal model is in rea-

sonable agreement with that of the measured profiles. Both the data and the model are roughly power law in nature, $\tau \simeq \dot{\gamma}^{0.2}$, although this is not exact. As a consequence, naïvely assuming a power-law fluid ($\tau_y = 0$, $\beta \approx 0.2$) captures the velocity profiles of Fig. 4 reasonably well (not shown), but *not* the rheometry in that figure’s inset. Only the nonlocal model resolves the apparent inconsistency between velocity profiles and rheometry.

Note that the nonlocal model does not capture the upward bend in the flow curves shown in Fig. 5a, which corresponds to regions roughly one bubble diameter from the shearing wall where the flow gradients are small — these are also responsible for the “misalignment” of the predicted and measured flow profiles seen in Fig. 5b.

Flows with a top plate. Here we compare predictions of the nonlocal model to flow in the presence of a top plate. We assume that the wall and bulk fluidities are unchanged from the case without a top plate and take $\xi/\langle d \rangle = 3$, the same parameters used in Figs. 5a and b. We include a

Bretherton wall drag $F_{bw} = c_{bw}|v|^{2/3}$, where $c_{bw} = 2.7 \times 10^5 \text{ Pa} \cdot \text{m}^{-5/3} \cdot \text{s}^{2/3}$ has been determined independently [12]. In Fig. 5c we compare flow profiles from the experiment and model. The model predictions are in surprisingly good agreement with experimental results. Rate dependence emerges, and the flow profiles are more localized than in the case absent a top plate.

Outlook. – We probed the flow profiles and rheology of two-dimensional foams in Couette geometries, both for foams squeezed below a top plate and for bubble rafts. Consistent with earlier experimental results in a linear geometry [12], flows below a top plate are strongly rate dependent. While for bubble rafts in a linear geometry one expects and finds rate independence [18,24], this is not to be expected in the Couette geometry, since a combination of a finite yield stress and a radial decay of the shear stress suggests a rate dependent location in the cell where the flow ceases [23,28]. Here we do not observe this effect: the velocity profiles for a wide range of strain rates collapse.

For bubble rafts, the local and global rheology do not match, and in particular the foam flows in regions where the stress is below the global yield stress. We can fit the flow profiles of both the bubble rafts and the confined foams by a nonlocal model that extends the measured Herschel-Bulkley rheology with an empirically determined length scale that captures the nonlocality.

We note that the effect of nonlocality for confined foams is not as strong as it is for the freely floating foams. Moreover, we suggest that the nonlocal effect would be even less important in the linear geometry, where a local model was found to capture the flow profiles [12]. Underlying this is that even the local model predicts no abrupt cessation of flow in linear geometry — and it is near such regions that the flow profiles are most sensitive to nonlocal effects.

One open question remains. If we assume the Herschel-Bulkley relation determined in the system with inner radius $r_i = 25 \text{ mm}$ also describes bubble raft in the system with $r_i = 105 \text{ mm}$, we can attempt to describe the velocity profiles in the large system using the nonlocal model. We obtain good agreement for a choice of cooperativity length $\xi/\langle d \rangle \approx 10$, significantly larger than that in the small system. We suggest that the radius of curvature may influence the cooperativity length in a way not captured in the model as presented here.

The authors wish to thank Anna Baas for experimental assistance and Jeroen Mesman for technical brilliance. It is a pleasure to thank Lyderic Bocquet and Wim van Saarloos for enlightening discussions. GK, BPT and MEM acknowledge funding by Stichting FOM.

REFERENCES

[1] HÖHLER R. and COHEN-ADDAD S., *J. Phys. Cond. Matt.*,

17 (2005) 1041.

[2] LACASSE M.-D., GREST G.S., LEVINE D., MASON T.G. and WEITZ, D.A., *Phys. Rev. Lett.*, **76** (1996) 3448.

[3] PRINCEN H.M., *J. Coll. Interf. Sci.*, **91** (1983) 160.

[4] BRETHERTON F.P., *J. Fluid Mech.*, **10** (1961) 166.

[5] AUSSILLOUS P. and QUÉRÉ, D. *Europhys. Lett.*, **59** (2002) 370.

[6] DENKOV N.D., SUBRAMANIAN V., GUROVICH D. and LIPS A., *Coll. Surf. A*, **263** (2005) 129.

[7] DENKOV N.D., TCHOLAKOVA S., GOLEMANOV K., SUBRAMANIAN V., and LIPS A., *Coll. Surf. A*, **282-283** (2006) 329.

[8] TERRIAC E., ETRILLARD J. and CANTAT I., *Europhys. Lett.*, **74** (2006) 909.

[9] DENKOV N.D., TCHOLAKOVA S., GOLEMANOV K., ANANTHAPADMANABHAN K.P. and LIPS A., *Phys. Rev. Lett.*, **100** (2008) 138301; TCHOLAKOVA S., DENKOV N.D., GOLEMANOV K., ANANTHAPADMANABHAN K.P. and LIPS A., *Phys. Rev. E*, **78** (2008) 011405.

[10] SAUGEY A., DRENCKHAN W. and WEAIRE D., *Phys. Fluids*, **18** (2006) 053101.

[11] LARSON R. G., *The Structure and Rheology of Complex Fluids* (Oxford University Press, New York) 1999.

[12] KATGERT G., MÖBIUS M.E. and VAN HECKE M., *Phys. Rev. Lett.*, **100** (2008) 058301.

[13] MÖBIUS M.E., KATGERT G. and VAN HECKE M., *arXiv:cond-mat.soft/0811.0534*.

[14] WANG Y., KRISHAN K. AND DENNIN M., *Phys. Rev. E*, **74** (2006) 041405.

[15] LAURIDSEN J., TWARDOS M. and DENNIN M., *Phys. Rev. Lett.*, **89** (2002) 098303.

[16] J.LAURIDSEN, G.CHANAN AND M. DENNIN, *Phys. Rev. Lett.*, **93** (2004) 018303.

[17] DEBRÉGEAS G., TABUTEAU H. and DI MEGLIO J.-M., *Phys. Rev. Lett.*, **87** (2001) 178305.

[18] WANG Y, KRISHAN K. and DENNIN M., *Phys. Rev. E*, **73** (2006) 031401.

[19] CLANCY R.J., JANIAUD E., WEAIRE D. and HUTZLER S., *Eur. Phys. J. E*, **21** (2006) 123.

[20] KRISHAN K. and DENNIN M., *Phys. Rev. E*, **78** (2008) 051504.

[21] CHEDDADI I., SARAMITO P., RAUFASTE C., MARMOTANT P. and GRANER F., *Eur. Phys. J. E*, **27** (2008) 123.

[22] KABLA A., SCHEIBERT J. and DEBREGEAS G., *J. Fluid Mech.*, **587** (2007) 45.

[23] DENNIN M., *J. Phys. Condens. Matter*, **20** (2008) 283103.

[24] JANIAUD E., HUTZLER S. and WEAIRE D., *Phys. Rev. Lett.*, **97** (2006) 038302.

[25] GOYON J., COLIN A., OVARLEZ G., AJDARI A. and BOCQUET L., *Nature*, **454** (2008) 84.

[26] BOCQUET L., COLIN A. and AJDARI A., *Phys. Rev. Lett.*, **103** (2009) 036001.

[27] RODTS S., BAUDEZ J.C. and COUSSOT P., *Europhys. Lett.*, **69** (2005) 636.

[28] GILBRETH C., SULLIVAN S. and DENNIN M., *Phys. Rev. E*, **74** (2006) 031401.

[29] ISA L., BESSELING R. and POON W.C.K., *Phys. Rev. Lett.*, **98** (2007) 198305.

[30] The integral $\int ds s^2 K(s)$ can be positive or negative. Real values of ξ correspond to the negative case. Imaginary ξ tends to produce non-monotonic velocity profiles.